

Journal of Materials Chemistry C

Accepted Manuscript



This is an *Accepted Manuscript*, which has been through the Royal Society of Chemistry peer review process and has been accepted for publication.

Accepted Manuscripts are published online shortly after acceptance, before technical editing, formatting and proof reading. Using this free service, authors can make their results available to the community, in citable form, before we publish the edited article. We will replace this *Accepted Manuscript* with the edited and formatted *Advance Article* as soon as it is available.

You can find more information about *Accepted Manuscripts* in the [Information for Authors](#).

Please note that technical editing may introduce minor changes to the text and/or graphics, which may alter content. The journal's standard [Terms & Conditions](#) and the [Ethical guidelines](#) still apply. In no event shall the Royal Society of Chemistry be held responsible for any errors or omissions in this *Accepted Manuscript* or any consequences arising from the use of any information it contains.

Schiff base derivatives containing heterocycle with aggregation-induced emission and recognition ability

Gang Liu^a, Mingdi Yang^{a, b, *}, Lianke Wang^a, Jun Zheng^c, Hongping Zhou^{a, *}, Jieying Wu^a, Yupeng Tian^a

Three new Schiff base derivatives possessing various blue-emitting aggregation-induced emission (AIE) characteristics in tetrahydrofuran (THF)/water were synthesized. The photophysical properties in solution, aqueous suspension, film and crystalline state, along with their relationships, are comparatively investigated. Crystallographic data of **dye 1** and **dye 3** indicate that the existence of multiple intermolecular hydrogen bonding interactions restricted the intramolecular vibration and rotation. Moreover, the size and growth process of particles with different water fractions were studied using a scanning electron microscope (SEM) and dynamic light scattering (DLS). The results show that the smaller and homogeneous particles assembling in an ordered fashion at appropriate water contents exhibited distinct AIE behavior. Moreover, in THF/H₂O (4:1, v:v) of HEPES (20 mM) buffer solution, **dye 2** illustrates the fluorescence turn-on sensing towards Cr³⁺ and Al³⁺ via chelation enhanced fluorescence (CHEF). The 2:1 stoichiometry of the sensor complexes (**dye 2**-Cr³⁺ and **dye 2**-Al³⁺) was calculated from Job plots based on fluorescence titrations.

www.rsc.org/materialsC

Introduction

The organic light-emitting materials led to a revolution in the field of optoelectronic devices and sensing. Design and synthesis of efficient light emitters in the solid and aggregate states are of importance to the development of advanced optical and biomedical devices, such as organic light-emitting diodes (OLEDs) and fluorescent biosensors.¹ However, most luminescence suffer from the problem of aggregation-caused quenching (ACQ)² due to strong π - π stacking interactions in the extended π -conjugated systems, which is a typical problem of common organic chromophores and thus limited their applications in real world which requires materials to be solid and phragmoid films.³

In the beginning of this century, Tang⁴ and Park,⁵ *et al.* have reported several material systems that have aggregation-induced emission (AIE) and aggregation-induced enhanced emission (AIEE) properties. AIE/AIEE luminescence is practically non-luminescent or weak emission in solution, but become strong emitters when aggregated as powders or nanoparticles or fabricated as solid thin films. In the past ten years, the AIE/AIEE mechanism were reported for the restriction of intramolecular rotation (RIR),⁶ twisted intramolecular charge transfer (TICT),⁷ *cis-trans* isomerisation,⁸ planarity and rotatability, *et al.*⁹ However, it seems that some of these mechanisms are conflicting and none of them can be used universally.¹⁰ So far, there is still much work to do to clarify the AIE behavior from the perspective of the molecular packing and electronic structure.

In our study, we synthesized a new series of Schiff bases with triphenylamine and benzimidazole groups (**dye 1-3**). Structurally, triphenylamine can not only increase the solubility of the molecule,

but also enhance the extent of electron delocalization and donating electron ability. Benzimidazole and C=N double bond groups are intended to enrich the π -electron density and increase the dimension of π -electron delocalization of the system. The molecules are a big conjugated system with twisted skeleton conformation, which may show good AIE characteristics. We aim to reveal the AIE features of these Schiff bases and structure-property relationship. The spectroscopic properties of these compounds in solution and crystal state were investigated to elucidate the mechanism of enhanced emission in the aggregation state. Moreover, development of fluorescent sensors for chemical species of biological and environmental significance is currently an attractive field for scientists.¹¹ Among fluorescence sensors, Schiff bases¹² are recognized as having simple synthetic steps and are applied to many optical sensors, as well as AIE applications.¹³ Considering these Schiff base compounds containing pyridine group, we evaluated the recognition abilities of three compounds with a range of metal ions. The **dye 2** was proved to be an efficient fluorescent sensor for metal ions.¹⁴

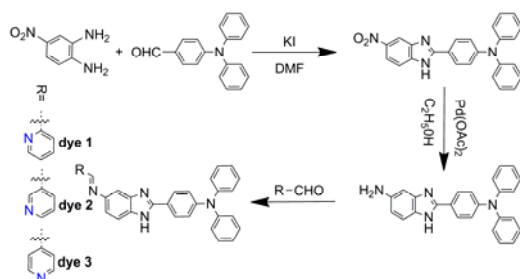
Experimental Section

Materials and apparatus

4-nitro-o-phenylenediamine, triphenylamine formaldehyde, Palladium acetate, 2-pyridinecarboxaldehyde, 3-pyridinecarboxaldehyde and 4-pyridinecarboxaldehyde were purchased from Aladdin, the other chemicals were available commercially and used without further purification. IR spectra were recorded with a FT-IR spectrometer (KBr discs) in the 4000-

400 cm^{-1} region. NMR spectra measurements were used at 400 MHz for ^1H NMR and 100 MHz for ^{13}C NMR, using $\text{DMSO}-d_6$ as solvent. Chemical shifts were reported in parts per million (ppm) relative to internal TMS (0 ppm) and coupling constants in Hz. Splitting Patterns were described as singlet (s), doublet (d), triplet (t), quartet (q), or multiple (m). The mass spectra were obtained on a LTQ Orbitrap XL mass spectrometer or autoflex speed MALDI-TOF/TOF mass spectrometer. The one-photon absorption (OPA) spectra were recorded on the UV-265 spectrophotometer. The one-photon excited fluorescence (OPEF) spectra measurements were performed using the Hitachi F-7000 fluorescence spectrophotometer. OPA and OPEF of **dye 1-3** were measured in THF with the concentration of 10 μM . The quartz cuvettes used were of 1 cm path length. Dynamic light scattering (DLS) measurements were conducted on a Delsa PN A54412AB Nano Submicron Grain Particle Size Analyzer. The scan electron microscopy (SEM) studies were performed using the Hitachi S-4800 scanning electron microscope. One drop of the solution or suspension was placed on a silicon slice, which was then dried in air.

Synthesis



Scheme 1 Synthetic routes to target dye 1-3.

Synthesis of 5-nitro-2-triphenylaminebenzimidazole

Triphenylamine formaldehyde (2.72 g, 10 mmol) and KI (0.2 g, 12 mmol) were added into 30 mL DMF of 4-Nitro-o-phenylenediamine. The mixture solution was refluxed at 150 $^{\circ}\text{C}$ for 120 h. The reaction was monitored by TLC. After the completing the reaction, the solution was cooled and added into water (500 mL). Filtrated and purified by column chromatography with petroleum (b.g 60-90 $^{\circ}\text{C}$)/ ethyl acetate (4:1) to give 3.94 g yellow solid, yield: 95%. ^1H -NMR (400 Hz, d_6 -DMSO, TMS): δ 13.36 (s, 1H), 8.41 (s, 1H), 8.07-8.12 (q, 3H, $J = 8.8$ Hz), 7.70-7.72 (d, 1H, $J = 8.0$ Hz), 7.31-7.41 (t, 4H, $J = 7.8$ Hz), 7.14-7.19 (q, 6H, $J = 7.6$ Hz), 7.04-7.06 (d, 2H, $J = 8.8$ Hz). ^{13}C -NMR (100 MHz, d_6 -DMSO, TMS): δ 149.69, 146.32, 142.38, 129.74, 128.20, 125.29, 124.29, 121.50, 120.75, 117.64. IR (KBr, cm^{-1}): 3051, 1642, 1593, 1471, 1343, 1172. ESI-MS (m/e): $[\text{M}]^+$ Calcd for $\text{C}_{25}\text{H}_{18}\text{N}_4\text{O}_2$ 406.15; Found 406.14.

Synthesis of 5-amino-2-triphenylaminebenzimidazole

5-amino-2-triphenylaminebenzimidazole (1.22 g, 3 mmol), hydrazine hydrate (15 mL) and palladium acetate (0.02 g, 0.8 mmol) were added to 50 mL ethanol under the protection of nitrogen, the mixture was refluxed for 1 h, cooled to room temperature. Filtrated and concentrated in vacuo. 1.0 g grey white solid was obtained by recrystallized from ethanol, yield: 95%. ^1H -NMR (400 MHz, d_6 -DMSO, TMS): δ 12.13 (s, 1H), 7.94-7.96 (d, 2H, $J = 8.4$ Hz), 7.34-7.37 (t, 4H, $J = 7.8$ Hz), 7.24-7.26 (s, 1H), 7.07-7.12 (q, 6H, $J = 6.8$ Hz), 7.01-7.03 (d, 2H, $J = 8.8$ Hz), 6.62 (s, 1H), 6.48-6.52 (s, 1H), 4.91 (s, 1H), 4.51 (s, 1H). ^{13}C -NMR (100 MHz, d_6 -DMSO, TMS):

δ 149.06, 148.04, 146.61, 144.53, 129.64, 127.00, 124.61, 123.80, 123.70, 121.91, 111.74. IR (KBr, cm^{-1}): 3455, 3382, 3196, 3051, 2598, 1632, 1576, 1488, 1333, 1277, 1172. ESI-MS (m/e): $[\text{M}]^+$ Calcd for $\text{C}_{25}\text{H}_{20}\text{N}_4$ 376.19; Found 376.15.

Synthesis of dye 1

2-Pyridinecarboxaldehyde (0.06 g, 0.55 mmol) was dropped into a solution of 5-amino-2-triphenylaminebenzimidazole (0.19 g, 0.5 mmol) dissolved in triethylamine (20 mL) and THF (2 mL). The solution was stirred for 2 h at room temperature. The reaction mixture was filtered, the yellow solid (0.21 g) was obtained, yield: 88%. ^1H -NMR (400 MHz, d_6 -DMSO, TMS): δ 12.85-12.86 (d, 1H, $J = 4.0$ Hz), 8.71-8.73 (d, 2H, $J = 5.2$ Hz), 8.19-8.21 (d, 1H, $J = 8.0$ Hz), 8.05-8.08 (d, 2H, $J = 8.0$ Hz), 7.95-7.98 (q, 1H, $J = 8.0$ Hz), 7.64-7.67 (d, 1H, $J = 8.0$ Hz), 7.52-7.54 (s, 1H), 7.48 (s, 1H), 7.36-7.40 (t, 4H, $J = 9.8$ Hz), 7.26-7.31 (q, 1H, $J = 8.0$ Hz), 7.12-7.16 (q, 6H, $J = 8.4$ Hz), 7.04-7.07 (d, 1H, $J = 8.4$ Hz). ^{13}C -NMR (100 MHz, d_6 -DMSO, TMS): δ 158.77, 158.50, 154.36, 152.43, 152.28, 149.59, 148.84, 146.57, 145.16, 144.86, 144.59, 143.51, 136.95, 135.59, 134.480, 129.75, 127.69, 125.28, 124.97, 123.99, 121.47, 118.86, 117.19, 116.34, 111.34, 110.49, 103.51. IR (KBr, cm^{-1}): 3414, 1593, 1544, 1399, 767, 686. MALDI-TOF m/z: $[\text{M}]^+$ Calcd for $\text{C}_{31}\text{H}_{23}\text{N}_5$ 465.11; Found 465.05.

Synthesis of dye 2

3-Pyridinecarboxaldehyde (0.06 g, 0.55 mmol) was dropped into a solution of 5-amino-2-triphenylaminebenzimidazole (0.19 g, 0.5 mmol) dissolved in triethylamine (20 mL) and THF (2 mL). The mixed solution was stirred for 2 h at room temperature. The reaction mixture was filtered, the yellow solid (0.20 g) was obtained, yield: 85%. ^1H -NMR (400 MHz, d_6 -DMSO, TMS): δ 12.82-12.83 (d, 1H, $J = 4.0$ Hz), 9.09-9.10 (d, 1H, $J = 4.0$ Hz), 8.82-8.83 (d, 1H, $J = 4.0$ Hz), 8.69-8.70 (d, 1H, $J = 4.0$ Hz), 8.33-8.36 (d, 1H, $J = 4.0$ Hz), 8.05-8.07 (d, 2H, $J = 8.4$ Hz), 7.61-7.66 (t, 1H, $J = 8.4$ Hz), 7.53-7.58 (s, 1H), 7.51 (s, 1H), 7.36-7.42 (q, 5H, $J = 8.8$ Hz), 7.23-7.36 (q, 1H, $J = 8.0$ Hz), 7.14-7.16 (q, 6H, $J = 8.8$ Hz), 7.05-7.07 (d, 2H, $J = 8.8$ Hz). ^{13}C -NMR (100 MHz, d_6 -DMSO, TMS): δ 162.29, 156.60, 156.27, 152.35, 152.12, 151.51, 150.27, 150.22, 148.80, 145.86, 145.53, 144.59, 143.19, 135.56, 134.75, 134.19, 131.84, 129.75, 127.66, 124.94, 123.98, 123.10, 121.50, 118.75, 117.26, 116.19, 110.17, 103.50, 103.40. IR (KBr, cm^{-1}): 3406, 3058, 1610, 1594, 1488, 1326, 1284, 694. MALDI-TOF m/z: $[\text{M}]^+$ Calcd for $\text{C}_{31}\text{H}_{23}\text{N}_5$ 465.11; Found 465.11.

Synthesis of dye 3

4-Pyridinecarboxaldehyde (0.06 g, 0.55 mmol) was dropped into a solution of 5-amino-2-triphenylaminebenzimidazole (0.19 g, 0.5 mmol) dissolved in (20 mL) methanol solution. The mixed solution was stirred for 24 h at room temperature. The reaction mixture was filtered, the yellow solid (0.20 g) was obtained, yield: 85%. ^1H -NMR (400 MHz, d_6 -DMSO, TMS): δ 12.88-12.89 (d, 1H, $J = 4.0$ Hz), 8.808 (s, 1H), 8.75-8.76 (d, 2H, $J = 4.0$ Hz), 8.06-8.08 (d, 2H, $J = 8.0$ Hz), 7.88-7.89 (d, 2H, $J = 4.0$ Hz), 7.27-7.32 (d, 1H, $J = 4.0$ Hz), 7.47-7.55 (d, 1H, $J = 4.0$ Hz), 7.36-7.40 (q, 4H, $J = 7.4$ Hz), 7.27-7.32 (t, 1H, $J = 4.0$ Hz), 7.12-7.16 (t, 6H, $J = 8.6$ Hz), 7.05-7.07 (d, 2H, $J = 8.0$ Hz). ^{13}C -NMR (100 MHz, d_6 -DMSO, TMS): δ 156.560, 156.65, 152.52, 152.45, 151.41, 150.47, 150.35, 148.84, 145.86, 145.53, 144.59, 143.19, 135.56, 134.75, 134.19, 131.84, 129.75, 127.66, 124.94, 123.98, 123.10, 121.50, 118.75, 117.26, 116.19, 110.17, 103.87. IR (KBr, cm^{-1}): 3406, 3058, 1610, 1594, 1488, 1326, 1284, 694. MALDI-TOF m/z: $[\text{M}]^+$ Calcd for $\text{C}_{31}\text{H}_{23}\text{N}_5$ 465.11; Found 465.22.

X-ray Crystallography

Data of single crystals were collected on a Siemens Smart 1000 CCD diffractometer. The determination of unit cell parameters and data collections were performed with Mo K α radiation ($\lambda = 0.71073$ Å). Unit cell dimensions were obtained with least-squares refinements, and all structures were solved by direct methods using SHELXS-97.¹⁵ The other non-hydrogen atoms were located in successive difference Fourier syntheses. The final refinement was performed by using full-matrix least-squares methods with anisotropic thermal parameters for non-hydrogen atoms on F^2 . The hydrogen atoms were added theoretically and processing parameters for **dye 1** and **dye 3** are shown in **Table 1**.

Table 1. Crystallographic Data for **dye 1** and **dye 3**.

compound	dye 1	dye 3
empirical formula	C ₆₂ H ₅₀ N ₁₀ O ₃	C ₃₁ H ₂₄ N ₅ O ₁
formula weight	983.12	482.55
crystal system	Monoclinic	Monoclinic
space group	<i>P2₁/c</i>	<i>P2₁/c</i>
<i>a</i> [Å]	16.824(5)	23.904(5)
<i>b</i> [Å]	27.111(5)	9.753(5)
<i>c</i> [Å]	11.546(5)	11.323(5)
β [°]	91.858(5)	98.054(5)
<i>V</i> [Å ³]	5264(3)	2613.18(19)
<i>Z</i>	4	4
<i>T</i> [K]	293(2)	298(2)
D _{calc} [g·cm ⁻³]	1.241	1.226
μ [mm ⁻¹]	0.079	0.077
θ range [°]	0.99-25.50	1.00-25.00
total no. data	38998	18153
no. unique data	9789	4610
no. params refined	894	342
<i>R</i> ₁	0.0726	0.0536
<i>wR</i> ₂	0.2111	0.1857
GOF	1.042	1.164

Results and discussion

Materials

Scheme 1 shows the synthesis routes of three compounds (**dye 1-3**). The experiment details and structure characterization data were described in the experimental section and supporting information. The key synthesis steps of the three compounds are aldehyde-ammonia condensation reaction. Schiff base can be readily obtained by 5-nitro-2-triphenylaminobenzimidazole and 2-pyridinecarboxaldehyde, 3-pyridinecarboxaldehyde or 4-pyridinecarboxaldehyde. The structures of the product molecules are confirmed by ¹H NMR, ¹³C NMR, mass spectral data (**Fig. S4-S18**) and X-ray crystallographic analysis.

Photophysical Properties

As shown in **Fig. 1**, **dye 1-3** display similar absorption spectra, which indicate that the position of the nitrogen atom in the molecule has almost no effect on the absorption. The relevant spectroscopic data are summarized in **Table S1**. In addition, the absorption spectra reveal distinct two absorption peaks, which were located at ~ 290 nm (λ_1) and ~ 374 nm (λ_2), respectively, the former is attributed to the π - π^* electronic transitions caused by the triphenylamine,¹⁶ whereas the latter is likely ascribed to π - π^* electronic transitions and ICT processes.¹⁷

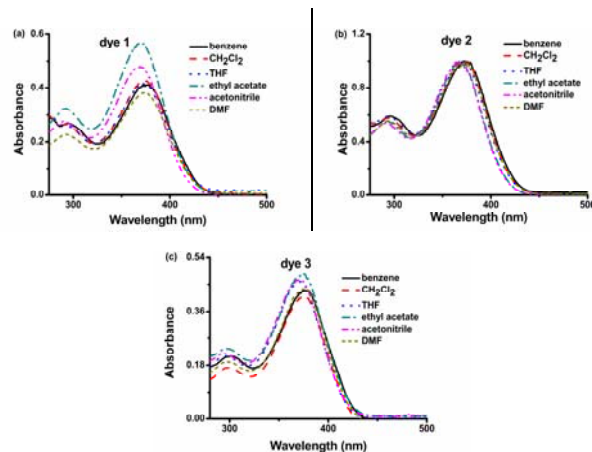


Fig. 1 Absorption spectra of **dye 1-3** in six organic solvents of different polarities with a concentration of 1.0×10^{-5} mol L⁻¹.

Aggregation-Induced Emission

The UV-vis spectrum of **dye 3** (10 μ M) with different water contents has been recorded and shown in **Fig. 2a**, we can see that **dye 3** show two absorption peaks in dilute THF solution. As water fraction (f_w) increases before reaches 90%, the peak at ~ 290 nm disappears gradually, and the peak at ~ 370 nm increases a litter and has a litter blue shift. As shown in **Fig. 2b**, the photoluminescence (PL) spectrum of **dye 3** in the THF/water mixture with different water contents shows that the PL intensity is very weak and observed almost no change as f_w increases from 0% to 20%. However, a significant enhancement of fluorescence is observed in the THF/water mixture with $f_w > 20\%$, accompanying with a small red-shift. The PL intensity in THF/water mixture with $f_w = 80\%$ is higher about 37.0 times than that in the pure THF solution. As $f_w = 90\%$, the PL intensity in THF/water mixture decreases respectively. Similar spectra changes are observed in the case of **dye 1** and **dye 2** (**Fig. S2**), thus we take **dye 3** as an example to explain the spectral changes.

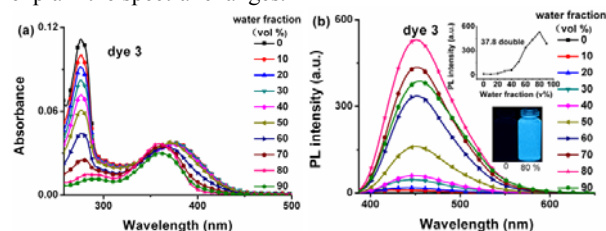


Fig. 2 (a) UV absorption spectra and (b) PL spectra changes of **dye 3** (1.0×10^{-5} mol L⁻¹) in THF/water mixtures with different water fractions.

The fluorescence quantum yields (Φ_F) values of **dye 1-3** in THF solution is nearly non-emissive and its Φ_F is $< 0.1\%$, they become stronger emitters in the aggregate state with Φ_F values up to 39%-47%. The experimental errors are estimated to be $\pm 10\%$ from sample concentrations and instruments. The PL decay dynamics of the compounds were studied by a time-resolved technique (**Table 2S**). The fluorescence decay behavior of **dye 1-3** in pure THF solution with the same concentration as that of the THF/water mixtures is well-fitted by the double-exponential, as show in **Fig. 3**, which were obtained by fitting the time-resolved fluorescence curves based on the following double-exponential function:

$$y = A_1 e^{-t/\tau_1} + A_2 e^{-t/\tau_2}$$

The values of A_1 and A_2 represent the fractional amount of molecules in each environment.¹⁸ With addition water fraction, the fluorescence lifetime gradually increase, when $f_w = 90\%$, the weighted mean time of **dye 3** (3.21 ns) is much longer than that of

in pure solvent (1.78 ns). The **dye 1** and **dye 2** have similar results (Table S2). This long lifetime indicates the existence of new aggregation species or couplings.¹⁹

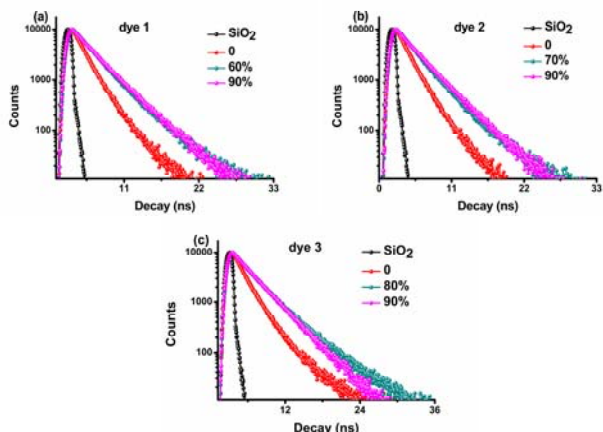


Fig. 3 Fluorescence lifetime of **dye 1-3** (1.0×10^{-5} mol L^{-1}) in THF/water mixture with different water fractions.

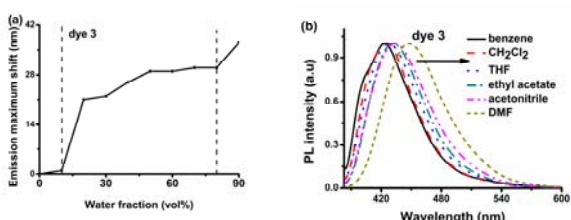


Fig. 4 (a) the change in the emission maximum peak of **dye 3** (1.0×10^{-5} mol L^{-1}) in THF/water mixtures with different water fractions. (b) PL spectra of **dye 3** in six organic solvents (1.0×10^{-5} mol L^{-1}).

As shown in Fig. 4a, with gradual addition of water to the THF, the maximum emission wavelength of **dye 3** is gradually redshifted about 40 nm, which is the same as the situation in different polar solvent (Fig. 4b). This is a typical TICT effect arising from the increased solvent polarity, here achieved by increasing the water fraction. Similar spectra changes also can be observed in **dye 1** and **dye 2** (Fig. S1, S3).

Crystal structure

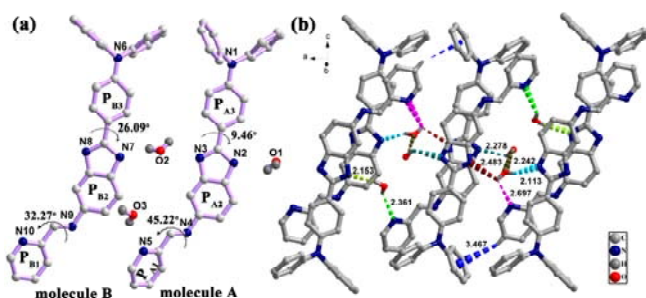


Fig. 5 (a) Molecular structure of **dye 1**; (b) The 1D chain of **dye 1** is formed by the O-H...N and C-H...π interactions.

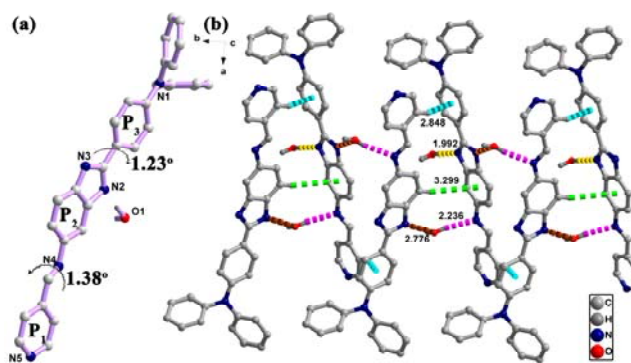


Fig. 6 (a) Molecular structure of **dye 3**; (b) The 1D chain of **dye 3** is formed by the O-H...N, O...N and C-H...π interactions.

In order to better understand the mechanism of AIE, we obtained single crystals of **dye 1** and **dye 3**. The relevant crystallographic data are summarized in Table 1. The dihedral angles between benzimidazole ring (P₂) and terminal pyridine ring (P₁), phenyl ring (P₃) of triphenylamine-based are 45.22° (P_{A1}-P_{A2}), 9.46° (P_{A2}-P_{A3}), 32.27° (P_{B1}-P_{B2}) and 26.09° (P_{B2}-P_{B3}) for **dye 1**, 1.38° (P₁-P₂) and 1.23° (P₂-P₃) for **dye 3**, respectively.

As shown in Fig. 5 and 6, the water molecules clutched tightly **dye 1** or **dye 3** molecule through multiple O-H...N and O...N bonds between N atoms of imidazole, pyridine and H, O atoms of H₂O with distances of 2.113 Å, 2.153 Å, 2.278 Å, 2.361 Å, 2.483 Å and 2.697 Å for **dye 1**, 1.922 Å, 2.236 Å and 2.776 Å for **dye 3**, respectively. Moreover, Fig. 5 and 6 show that **dye 1** and **dye 3** also restricted by several kinds of C-H...π hydrogen bond ($d = 3.467$ Å for **dye 1**, $d = 2.848$ Å and $d = 3.299$ Å for **dye 3**). The interactions fix the benzimidazole, pyridine and triphenylamine, which further prevent the free rotation around the C-C single bonds. Then, the molecule becomes more rigid. We can infer that the intramolecular motion is strongly restricted with increasing the water fraction in THF solution of dyes. As for the PL intensity of **dye 1-3** very weak in the film and crystalline state, the causes are still not very clear. It's likely formed excimers²⁰ or other morphologies of the aggregates.

Scanning electron microscope (SEM) and Dynamic light scattering (DLS)

In order to further probe with enhanced emission of **dye 1-3** in THF/water, we use scanning electron microscope (SEM) and dynamic light scattering (DLS) to examine the morphological structure and average diameter of different volume fractions of **dye 1-3** (Fig. 7, 8 and Table S3). SEM of **dye 2** in THF/water mixture with $f_w = 70\%$ shows a smaller and homogeneous crystalline state with the average diameter of 193 nm by DLS. However, when f_w reaches 90%, some larger and asymmetric crystalline particles are formed with the average diameter of 659 nm. Moreover, with the time change, the aggregates form the smaller and homogeneous particles step by step, as shown in Fig. 9. This phenomenon suggests that the diameters of the particles are correlated with the THF/water ratio. This result gave us the direct evidence of molecular aggregation during the emission enhancement, smaller and homogeneous particles in THF/water is in favor of fluorescence emissions.²¹

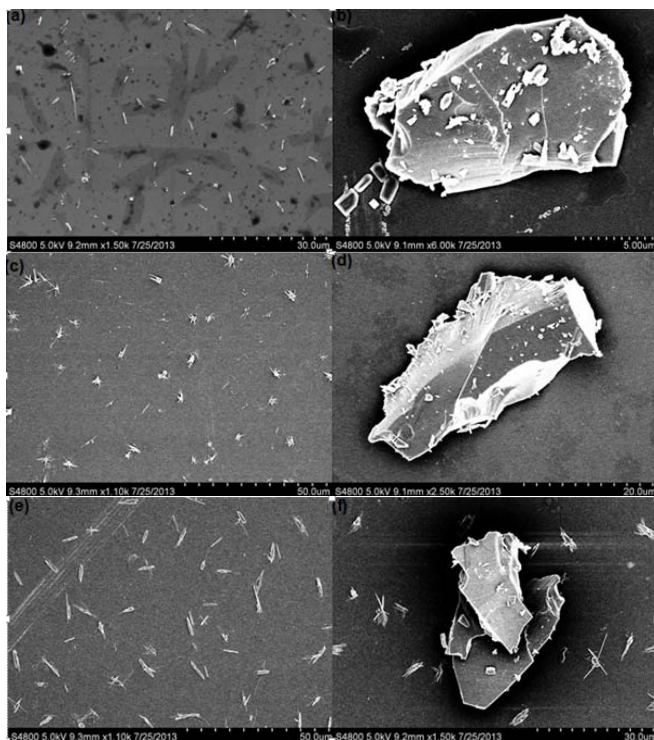


Fig. 7 SEM images of **dye 1-3** in THF/water mixtures at concentration of 1.0×10^{-5} M with different water fractions: (a) **dye 1** in THF/water (40/60, v/v); (b) **dye 1** in THF/water (10/90, v/v); (c) **dye 2** in THF/water (30/70, v/v); (d) **dye 2** in THF/water (10/90, v/v); (e) **dye 3** in THF/water (20/80, v/v); (f) **dye 3** in THF/water (10/90, v/v).

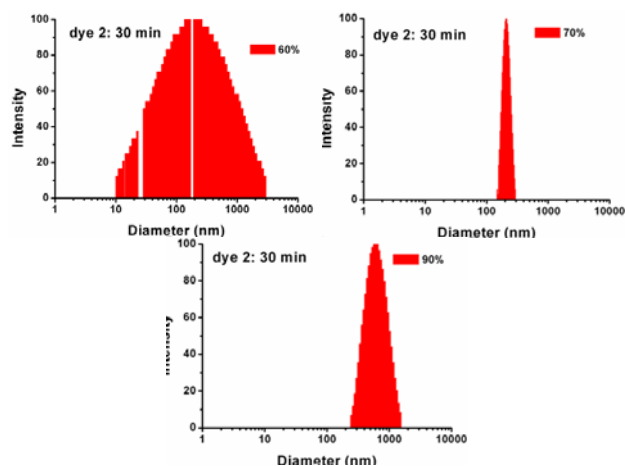


Fig. 8 Particle size distributions of **dye 2** in THF/water mixture with 50%, 60%, and 90% of water fractions.

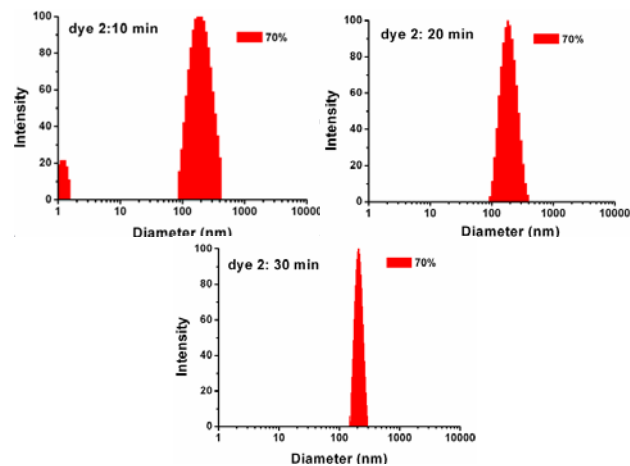


Fig. 9 Particle size distributions of **dye 2** in 70% water fraction at time of 10 min, 20 min, and 30 min.

Electronic structure

To better understand the photophysical properties of the present luminogens, theoretical calculations on their energy levels were performed. The molecular orbital amplitude plots of the highest occupied molecular orbitals (HOMOs) and the lowest unoccupied molecular orbitals (LUMOs) of **dye 1-3** are shown in **Fig. 10**. The electrons of the compounds' HOMOs are confined mainly on the TPA and benzimidazole moiety, while LUMOs+1 are distributed mainly on the benzimidazole moiety.

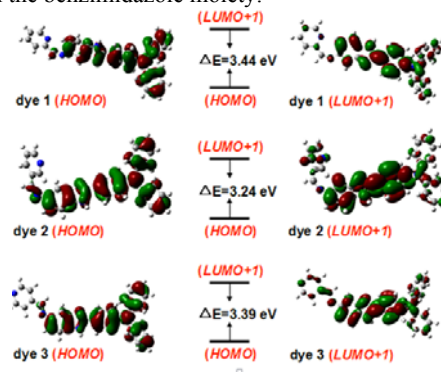


Fig. 10 Energy level and electron density distribution of frontier molecular orbital of **dye 1-3**.

Recognition toward metal ions

We evaluated sensor properties of these triphenylamine-substituted benzimidazole-based conjugated Schiff bases. The cation binding properties of the chemosensors were studied by employing the nitrate salts of Ag^+ , Ba^{2+} , Ca^{2+} , Cd^{2+} , Co^{2+} , Cu^{2+} , K^+ , Hg^{2+} , Pd^{2+} , Mg^{2+} , Li^+ , Na^+ , Ni^{2+} , Zn^{2+} , Fe^{3+} , Cr^{3+} , Al^{3+} , Ce^{2+} , Mn^{2+} , Se^{2+} , Fe^{2+} . By studying comparatively, **dye 2** has a special sensor for Cr^{3+} and Al^{3+} . However, **dye 1** and **dye 3** have enhanced fluorescence for numerous ions. As showed in **Fig. 11**, **dye 2** shows better selectivity to Cr^{3+} and Al^{3+} , the PL intensity of **dye 2**+ Cr^{3+} and **dye 2**+ Al^{3+} increase by 10 and 11 fold, respectively. To further understanding the interactions between **dye 2**- Cr^{3+} and **dye 2**- Al^{3+} , fluorescence spectrum of **dye 2** in THF/ H_2O (4:1, v/v), HEPES (20 mM) buffer solution titrated with Al^{3+} and Cr^{3+} be obtained. As shown in **Fig. 12**, the PL intensity was increased progressively. To understand the nature of interactions between sensor and metal ions, Job's plot tests were carried out. As seen in **Fig. 13**, the results indicated 2:1 stoichiometric complexation of **dye 2** in buffer

solution with Al^{3+} and Cr^{3+} , respectively. In addition, the association constants for Al^{3+} and Cr^{3+} are 1.27×10^5 and 1.01×10^5 , respectively. According to the Levenberg-Marquardt algorithm, considering the influence C=N and pyridine, the structure of **dye 1-3** have good chelation activity. Therefore, the possible reason can be explained *via* chelation enhanced fluorescence.²²

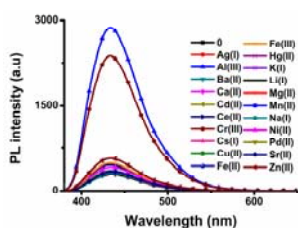


Fig. 11 Fluorescence spectra of **dye 2** (1.0×10^{-5} M, THF) upon addition of 1 equiv of different nitrate salts in 4:1 (v/v) THF/water HEPES buffer solution.

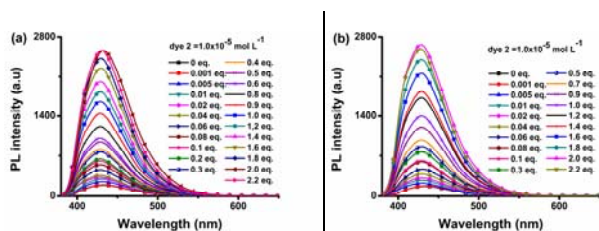


Fig. 12 Changes in the fluorescence spectrum of **dye 2** in THF/ H_2O (4:1, V/V), HEPES (20 Mm) buffer solution upon titration with aqueous solution of Al^{3+} (a) and Cr^{3+} (b).

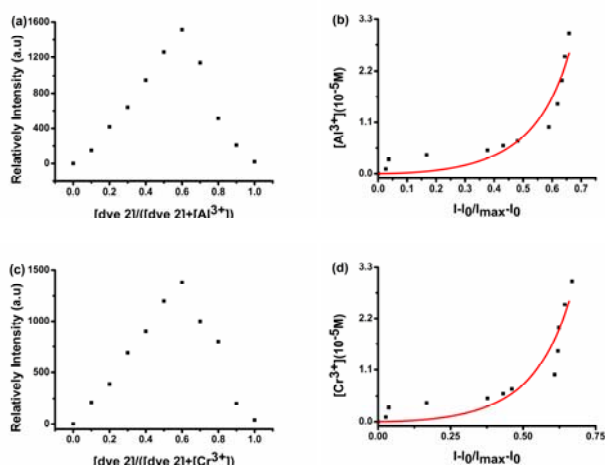


Fig. 13 (a) Job's plot of **dye 2** and Al^{3+} ($\lambda = 370$ nm). The total concentration of **dye 2** and Al^{3+} are 1.0×10^{-5} M. The experiments were measured at room temperature in THF. (b) Levenberg-Marquardt algorithm plot of the **dye 2**- Al^{3+} complex at room temperature in THF. (c) Job's plot of **dye 2** and Cr^{3+} ($\lambda = 370$ nm). The total concentration of **dye 2** and Cr^{3+} are 1.0×10^{-5} M. The experiments were measured at room temperature in THF. (d) Levenberg-Marquardt algorithm plot of the **dye 2**- Cr^{3+} complex at room temperature in THF.

To verify the selectivity of the present approach towards Al^{3+} and Cr^{3+} analysis, control experiments were conducted under the same experimental conditions as those involved for the Al^{3+} or Cr^{3+} , respectively. As showed in **Fig. 14**, **dye 2** recognized Al^{3+} and Cr^{3+} in a deal manner with little interference.

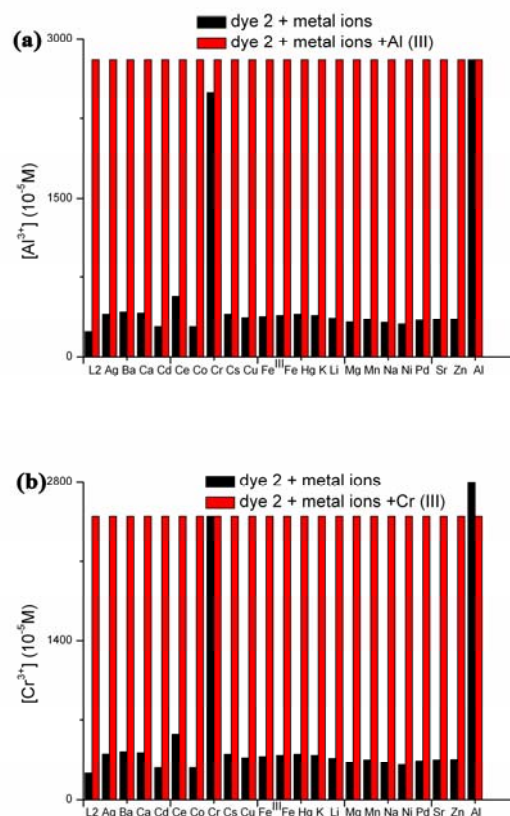


Fig. 14 (a) the results of interfere tests of **dye 2**- Al^{3+} in THF/ H_2O (4:1, v/v) respectively. The low bars represent **dye 2** (1.0×10^{-5} M) with cations (1.0×10^{-5} M) except for Al^{3+} ; the high bars represent **dye 2** (1.0×10^{-5} M) with cations (1.0×10^{-5} M) upon the subsequent addition of Al^{3+} (1.0×10^{-5} M). (b) the results of interfere tests of **dye 2**- Cr^{3+} in THF/ H_2O (4:1, v/v) respectively. The low bars represent **dye 2** (1.0×10^{-5} M) with cations (1.0×10^{-5} M) except for Cr^{3+} ; the high bars represent **dye 2** (1.0×10^{-5} M) with cations (1.0×10^{-5} M) upon the subsequent addition of Cr^{3+} (1.0×10^{-5} M).

Conclusions

In summary, we have obtained three triphenylamine-substituted benzimidazole-based conjugated Schiff bases. Crystal structure, SEM and DSL analysis revealed that the smaller and homogeneous particles caused by different water fractions play an important role in AIE behavior. In addition, in THF/ H_2O (4:1, v/v) HEPES (20 mM) buffer solution, **dye 2** exhibits a strong affinity of Al^{3+} , Cr^{3+} with the fluorescence totally enhanced compared to other metal ions.

Acknowledgment

This work was supported by the Program for New Century Excellent Talents in University (China), the Doctoral Program Foundation of the Ministry of Education of China (20113401110004), the National Natural Science Foundation of China (21271003, 21271004 and 51372003), the Natural Science Foundation of Education Committee of Anhui Province (KJ2012A024), the 211 Project of Anhui University, Higher Education Revitalization Plan Talent Project of (2013) and the Ministry of Education Funded Projects Focus on Returned Overseas Scholar.

Notes and References

^aCollege of Chemistry and Chemical Engineering, Anhui University and Key Laboratory of Functional Inorganic Materials Chemistry of Anhui Province, Hefei 230601, P. R. China.

^bSchool of Materials and Chemical Engineering, Anhui Jianzhu University, Hefei 230601, P. R. China.

^cCenter of Modern Experimental Technology, Anhui University, Hefei 230039, P. R. China.

*Corresponding author. ^aFax: +86-551-63861279, Tel: +86-551-63861279;

^bFax: +86-551-63828106, Tel: +86-551-63828150.

Crystallographic data have been deposited with the Cambridge Crystallographic Data Centre as supplementary publication no. CCDC: 932875, 941787.

Electronic Supplementary Information (ESI) available: **Fig.S4-S18**, Tables S1-S3.

- (a) K. Komatsu, Y. Urano, H. Kojima, T. Nagano, *J. Am. Chem. Soc.*, 2007, **129**, 13447-13454; (b) W. B. Cai, D. W. Shin, K. Gheysens, O. Cao, S. X. Wang, S. S. Gambhir, X. Y. Chen, *Nano. Lett.*, 2006, **6**, 669-676; (c) S. R. Forrest, *Nature* 2004, **428**, 911-918; (d) Y. Q. Tian, C. Y. Chen, C. C. Yang, A. C. Young, S. H. Jang, W. C. Chen, A. K. Y. Jen, *Chem. Mater.*, 2008, **20**, 1977-1987; (e) W. B. Cai, D. W. Shin, K. Chen, O. Gheysens, Q. Cao, S. X. Wang, S. S. Gambhir, X. Y. Chen, *Nano. Lett.*, 2006, **6**, 669-676.
- (a) S. W. Thomass III, G. D. Joly, T. M. Swager, *Chem. Rev.*, 2007, **107** 1339-1386; (b) C. T. Chen, *Chem. Mater.*, 2004, **16**, 4389-4400; (c) J. B. Birks, *Photophysics of Aromatic Moelcules*; Wiley & Sons: London, 1970.
- (a) E. A. Jares-Erijman, T. M. Jovin, *Nat. Biotechnol.*, 2003, **21**, 1387-1395; (b) H. Saigusa, E. C. Lim, *J. Phys. Chem.*, 1995, **99**, 15738-15747; (c) Y. Q. Dong, J. W. Y. Lam, A. J. Qin, Z. Li, J. Z. Sun, H. H. Y. Sung, I. D. Williams, B. Z. Tang, *Chem. Commun.* 2007, 40-42.
- (a) J. Luo, Z. Xie, J. W. Y. Lam, L. Cheng, H. Chen, C. Qiu, H. S. Kwok, X. Zhan, Y. Liu, D. Zhu, B. Z. Tang, *Chem. Commun.*, 2001, **18**, 1740-1741; (b) J. Chen, C. C. W. Law, J. W. Y. Lam, Y. Dong, S. M. F. Lo, I. D. Williams, D. Zhu, B. Z. Tang, *Chem. Mater.*, 2003, **15**, 1535-1546; (c) Z. Li, Y. Q. Dong, B. X. Mi, Y. H. Tang, M. Häussler, H. Tong, Y. Q. Dong, Jacky W. Y. Lam, Y. Ren, Herman H. Y. Sung, Kam S. Wong, P. Gao, Ian D. Williams, H. S. Kwok, and B. Z. Tang, *J. Phys. Chem. B.*, 2005, **109**, 10061-10066.
- B. K. An, S. K. Kwon, S. D. Jung, S. Y. Park, *J. Am. Chem. Soc.*, 2002, **124**, 14410-14415.
- (a) Y. P. Li, F. Li, H. Y. Zhang, Z. Q. Xie, W. J. Xie, H. Xu, B. Li, F. Y. Z. Shen, L. M. Hanif, *Chem. Commun.*, 2007, **3**, 231-233; (b) Q. Zeng, Z. Li, Y. Dong, C. Di, A. Qin, Y. Hong, Z. Zhu, C. K. W. Jim, G. Yu, Q. Li, Z. A. Li, Y. Liu, J. Qin, B. Z. Tang, *Chem. Commun.*, 2007, **1**, 70-71; (c) Z. P. Yu, Y. Y. Duan, L. H. Cheng, Z. L. Han, Z. Zheng, H. P. Zhou, J. Y. Wu, Y. P. Tian, *J. Mater. Chem.*, 2012, **22**, 16927-16932.
- (a) R. R. Hu, E. Lager, A. Aguilar-Aguilar, J. Z. Liu, J. W. Y. Lam, H. H. Y. Sung, I. D. Williams, Y. C. Zhong, K. S. Wong, E. Pena-Cabrera, B. Z. Tang, *J. Phys. Chem. C.*, 2009, **113**, 15845-15853; (b) Y. Qian, M. M. Cai, L. H. Xie, G. Q. Yang, S. K. Wu, W. Huang, *ChemPhysChem.*, 2011, **12**, 397-404; (c) Y. Qian, M. M. Cai, X. H. Zhou, Z. Q. Gao, X. P. Wang, Y. Z. Zhao, X. H. Yan, W. Wei, L. H. Xie, W. Huang, *J. Phys. Chem. C.*, 2012, **116**, 12187-12195.
- Z. Q. Xie, B. Yang, G. Cheng, L. L. Liu, F. He, F. Z. Shen, Y. G. Ma, S. Y. Liu, *Chem. Mater.*, 2005, **5**, 1995-1964.
- (a) Y. Yamaguchi, Y. Matsubara, T. Ochi, T. Wakamiya, Z. I. Yoshida, *J. Am. Chem. Soc.*, 2008, **130**, 13867-13869; (b) A. Loudet, K. Burgess, *Chem. Rev.*, 2007, **107**, 4891-4932; (c) R. Kabe, H. Nakanotani, T. Sakanoue, M. Yahiro, C. Adachi, *Adv. Mater.*, 2009, **21**, 4034-4038; (d) M. Shimizu, H. Tatsumi, K. Mochida, K. Shimono, T. Hiyama, *Chem. Asian J.*, 2009, **4**, 1289-1297.
- (a) Y. M. You, H. S. Huh, K. S. Kim, S. W. Lee, D. H. Kim, S. Y. Park, *Chem. Commun.*, 2008, **34**, 3998-4000; (b) Z. Zhen, H. P. Zhou, G. Y. Xu, Z. P. Yu, X. F. Yang, L. H. Cheng, L. Kong, Y. Feng, J. Y. Wu, Y. P. Tian, *Tetrahedron.*, 2012, **68**, 6569-6574.
- (a) S. W. Thomas, G. D. Joly, T. M. Swager, *Chem. Rev.*, 2007, **107**, 1339-1386; (b) P. Jiang, Z. Guo, *Coord. Chem. Rev.*, 2004, **248**, 205-229; (c) R. Martinez-Mannez, F. Sancenon, *Chem. Rev.*, 2003, **103**, 4419-4476; (d) Q. Zhao, F. Li, C. Huang, *Chem. Soc. Rev.*, 2012, **41**, 3210-3244.
- (a) V. Bhalla, R. Tejpal, R. Kumar, A. Sethi, *Inorg. Chem.*, 2009, **48**, 11677-11684; (b) D. Maity, A. K. Manna, D. Karthigeyan, T. K. Kundu, S. K. Pati, T. Govindarju, *Chem.-Eur. J.*, 2011, **17**, 11152-11161; (c) S. Sumalekshmy, C. J. Fahrni, *Chem. Mater.*, 2011, **23**, 483-500; (d) D. Maity, T. Govindaraju, *Inorg. Chem.*, 2011, **50**, 11282-11284; (e) J. F. Jang, Y. Zhou, J. Yoon, J. S. Kim, *Chem. Soc. Rev.*, 2011, **40**, 3416-3429.
- (a) M. Kumar, R. Kumar, V. Bhalla, *Org. Lett.*, 2011, **13**, 366-369; (b) K. H. Chen, J. S. Yang, C. Y. Hwang, M. Feng, *Org. Lett.*, 2008, **10**, 4401-4404; (c) L. Basabe-Desmonts, D. N. Reinhoudt, M. Crego-Calama, *Chem. Soc. Rev.*, 2007, **36**, 993-1017; (d) J. M. Kim, S. J. Min, S. W. Lee, J. H. Bok, J. S. Kim, *Chem. Commun.*, 2005, 3427-3429.
- (a) X. Y. Zhang, X. Q. Zhang, B. Yang, S. Q. Wang, M. Y. Liu, Y. Zhang, L. Tao, and Y. Wei, *RSC Adv.*, 2013, **3**, 9633-9636; (b) X. Q. Zhang, X. Y. Zhang, S. Q. Wang, M. Y. Liu, L. Tao, and Y. Wei, *Nanoscale.*, 2013, **5**, 147-150.
- G. M. Sheldrick, *SHELXTL V5.1 Software Reference Manual*, Bruker AXS, Inc., Madison, Wisconsin, USA, 1997.
- H. B. Xiao, C. Mei, Y. C. Wang, H. Li, S. X. Qian, H. Y. Yin, Z. S. Xu, *Materials Chem. Physics.*, 2011, **130**, 897-902.
- (a) S. J. Chung, T. C. Lin, Kim. K. S, G. S. He, J. Swiatkiewicz, P. N. Prasad, G. A. Baker, F. V. Bright, *Chem. Mater.*, 2001, **13**, 4071-4076; (b) H. J. Lee, J. Sohn, J. Hwang, S. Y. Park, *Chem. Mater.*, 2004, **16**, 456-465.
- R. Yan, Jacky. W. Y. Lam, Y. Q. Dong, B. Z. Tang, K. S. Wong, *J. Phys. Chem. B.*, 2005, **109**, 1135-1140.
- L. Li, Y. P. Tian, J. X. Yang, P. P. Sun, J. Y. Wu, H. P. Zhou, S. Y. Zhang, B. K. Jin, X. J. Xing, C. K. Wang, M. Li, G. H. Cheng, H. H. Tang, W. H. Huang, X. T. Tao, M. H. Jiang, *Chem.-Asian J.*, 2009, **4**, 668-703.
- Y. Q. Dong, J. W. Y. Lam, A. J. Qin, Z. Li, J. Z. Sun, H. H. Y. Sung, I. D. Williams, and B. Z. Tang, *Chem. Commun.*, 2007, **1**, 40-42.
- J. Wang, J. Mei, R. Hu, J. Z. Sun, A. Qin, B. Z. Tang, *J. Am. Chem. Soc.*, 2012, **134**, 9956-9966.
- (a) S. Goswami, D. Sen, N. K. Das, *Org. Lett.*, 2009, **12**, 856-859; (b) K. Soojin, Y. N. Jin, Y. K. Ka, H. K. Jin, K. K. Hee, N. Seong-Won, H. K. So, P. Sungsu, K. Cheal, K. Jinheung, *Inorg. Chem.*, 2012, **51**, 3597-3602; (c) R. Joseph, C. P. Rao, *Chem. Rev.*, 2011, **111**, 4658-4702.

